Electronic Supplementary Information (ESI)

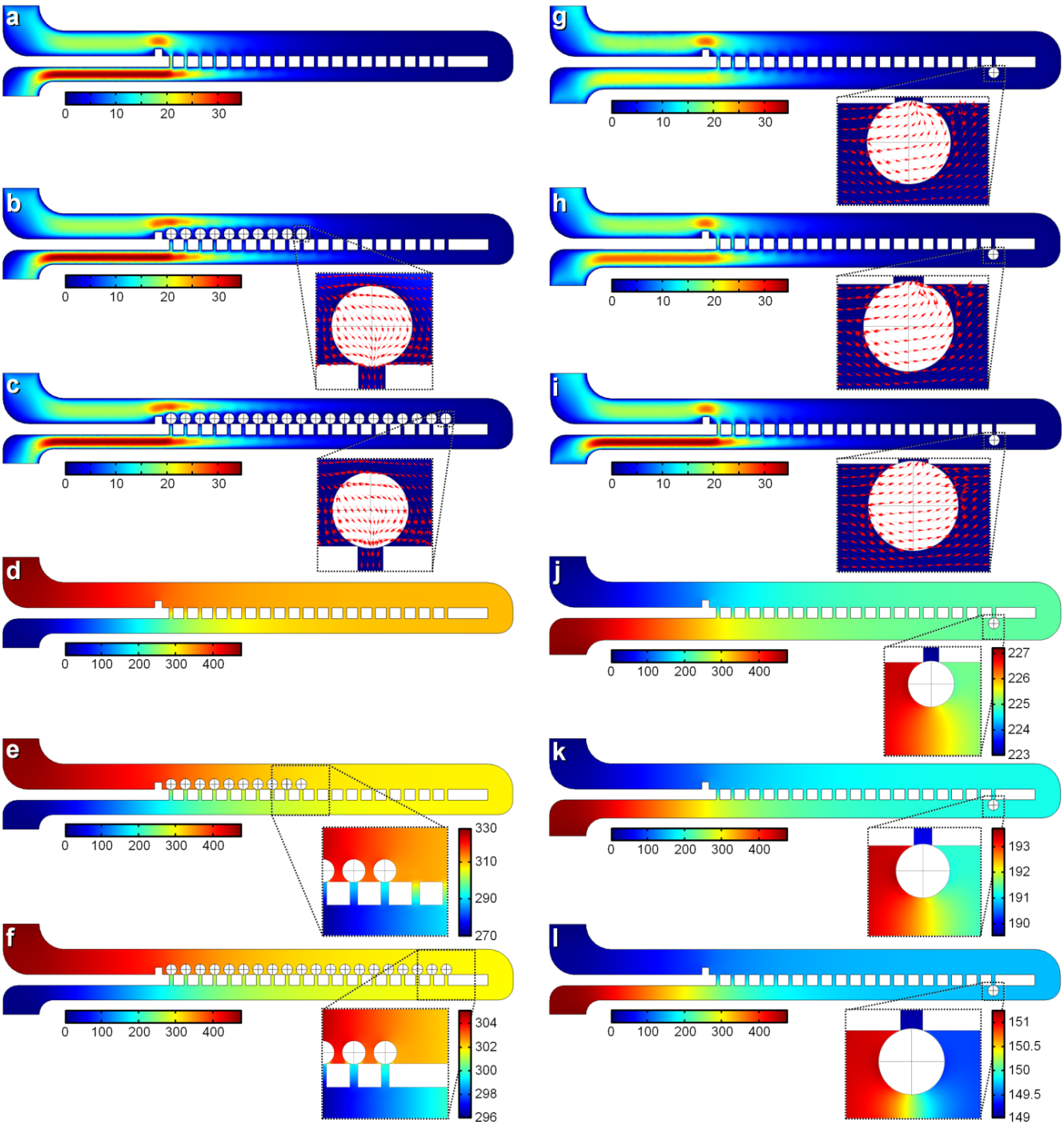

ESI Fig. 1 Three-dimensional COMSOL Multiphysics simulation results for the resettable micropost array trapping (μPAT) system. (a-c) Sequential fluid velocity field simulations for μPAT systems with zero (a), ten (b), and 20 (c) trapped microbeads under forward fluidic flow. The trapping width (W_T) and resetting width (W_R) are 35 μm and 20 μm, respectively. (d-f) Sequential pressure field simulations for μPAT systems with zero (d), ten (e), and 20 (f) trapped microbeads under forward fluidic flow. W_T = 35 μm; W_R = 20 μm. (g-i) Fluid velocity field simulations for μPAT systems with one microbead located at the back of the last trapping site under reverse fluidic flow. W_T = 35 μm; W_R = (g) 30 μm, (h) 25 μm, and (i) 20 μm. (j-l) Pressure field simulations for μPAT systems with one microbead located at the back of the last trapping site under reverse fluidic flow. W_T = 35 μm; W_R = (j) 30 μm, (k) 25 μm, and (l) 20 μm. Units for the velocity fields and pressure fields are mm s^{-1} and Pa, respectively. The overlaid red arrows in the expanded views (b, c, g-i) mark the directions of the fluid velocity fields at seven different heights.

Three-dimensional fluid velocity field and pressure field simulations were performed using the commercial finite element analysis software, COMSOL Multiphysics version 3.5a. Rigid spheres (15 μm in diameter) were used to model the microparticles. The three-dimensional "Incompressible Navier–Stokes" application mode for steady-state analysis was used for all simulations. For the velocity field simulations, the inputted fluid velocity was set at 7.0 mm s^{-1}. For the pressure field simulations, the inputted pressure was set at 480 Pa. For all of the simulations, the output pressure was set at 0 Pa, while all other boundary conditions were set to have no-slip conditions. The mesh size was refined to ensure that the simulation results were independent of mesh size. All simulations included mesh sizes of $1.2\times10^5 \pm 0.5\times10^5$ elements. Water ($\rho = 10^3$ kg m^{-3}; $\eta = 10^{-3}$ Pa•s) was modelled in all of the fluidic simulations.

ESI Fig. 1a-f show the changes in the flow dynamics within the resettable μPAT system at different points during the microparticle arraying process. For fluid flow through the trapping channels, the fluid velocity and pressure drop are highest for the first trapping site, decreasing sequentially until the final trapping position (ESI Fig. 1a, d). These results suggest that inputted microparticles would be preferentially transported to the earlier vacant trapping sites instead of the latter array positions. After microparticles immobilize in the first ten traps, the fluid velocity and pressure drop remain highest for the first trapping site; however, due to the microparticles obstructing fluid flow through the trapping channels, fluid flow is diverted to the remaining vacant trapping sites (ESI Fig. 1b, e). This flow behaviour is consistent for the resettable μPAT system with microparticles arrayed in each trapping location, with the exception that fluid flow in this case is instead partially diverted to bypass the occupied trapping sites (ESI Fig. 1c, f). After microparticles are arrayed in the trapping positions, the spherical particles do not fully block the fluid flow through the rectangular trapping channels (ESI Fig. 1b, c – *expanded views*). This residual flow could be reduced by using trapping channels with circular-shaped cross-sectional areas (*e.g.*, to enable higher numbers of particles to be arrayed in parallel); however, constructing circular channels would significantly increase the cost, time, and labor associated with device fabrication.

ESI Fig. 1g-l provide insight into the effects of decreasing the channel size (*i.e.*, reducing W_R) on the flow patterns surrounding microparticles located at the backs of the trapping sites. Specifically, the expanded views of the velocity fields in ESI Fig. 1g-i show that as W_R is decreased, higher proportions of the fluid velocity vectors (*red arrows*) are oriented perpendicular to the trapping channel (*i.e.*, in the *rightward* direction), particularly in the *top right* quadrant of the particle. This is in stark contrast to the expanded views from ESI Fig. 1b and c, where the majority of the velocity vectors surrounding the trapped microparticles are directed into the trapping channel. Similarly, reducing W_R was also found to increase the ratio of the pressure drop in the direction perpendicular to the trapping channel over the pressure drop through the channel (ESI Fig. 1d, e, j-l – *expanded views*). The resettable μPAT system with $W_R = 20$ μm was the only simulation in which the pressure drop perpendicular to the trapping channel was larger than the pressure drop across the microbead and through the trap (ESI Fig. 1l). These results suggest that decreasing W_R would deter microparticle immobilization at the backs of trapping sites during experimental runs, thereby improving resettability performance.

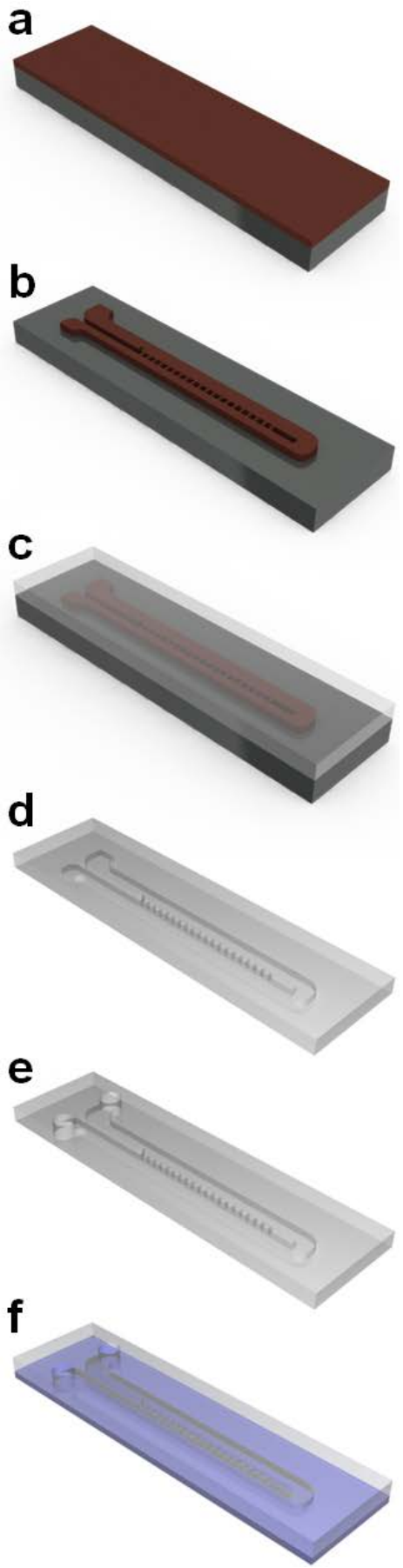

ESI Fig. 2 Microdevice fabrication process. (a) The negative photoresist, SU-8 2010 (MicroChem, Newton, MA), was spin-coated onto standard 4" Silicon wafers. (b) Microfeatures were defined *via* contact photolithography (Hybralign, Series 400, Optical Associates, Milpitas, CA). (c) Using the developed photoresist as a negative master, the device was micromolded with the silicone elastomer, poly(dimethylsiloxane) (PDMS), at a 10:1 (base : curing agent) ratio (Sylgard 184, Dow Corning, Corning, NY). (d) After curing at 55 °C for at least two hours, the PDMS was removed and individual devices were cut from the PDMS. (e) Ports for the catheter couplers (Instech Laboratories, Plymouth Meeting, PA) were punched at inlet and outlet locations. (f) The PDMS devices were cleaned and covalently bonded to Fisherbrand glass microscope slides (Fisher Scientific, Pittsburgh, PA) *via* UV ozone treatment (UVO cleaner, model 42, Jetlight Company, Irvine, CA).

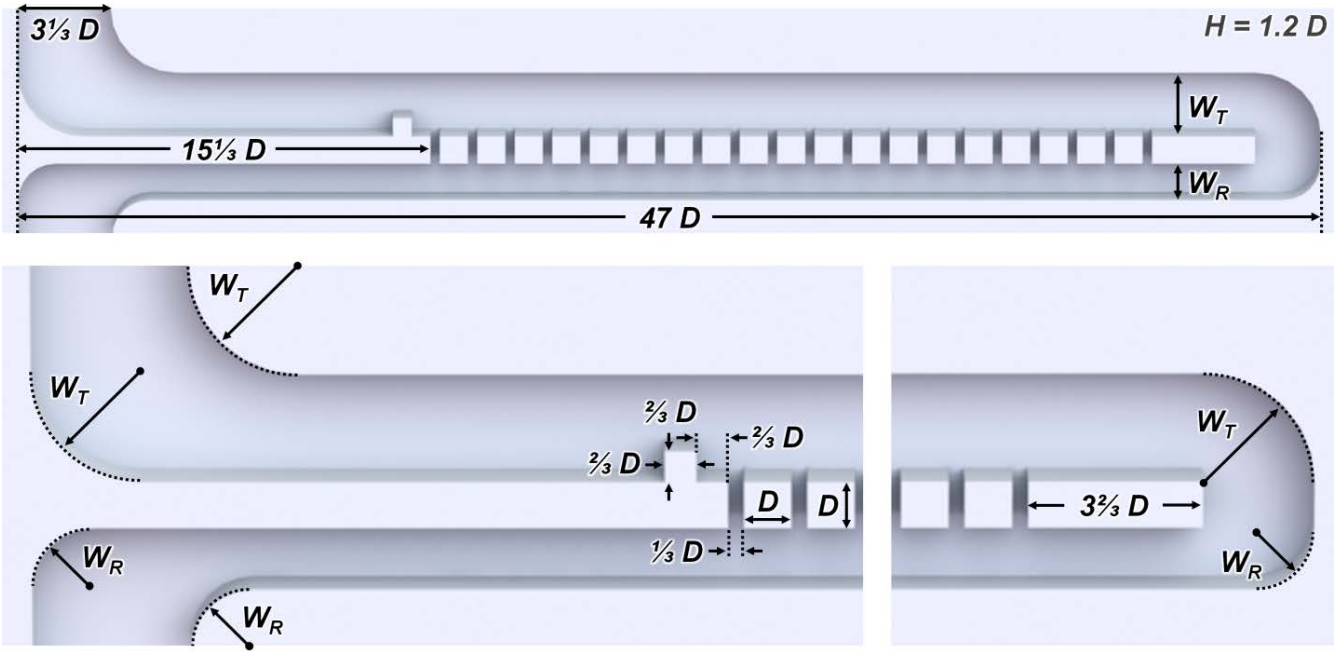

ESI Fig. 3 Design guidelines for the resettable μPAT system in terms of the diameter (D) of the target microparticles. $W_T = 2⅓\ D$; $W_R = 1⅓\ D$; H is the uniform height of the system.

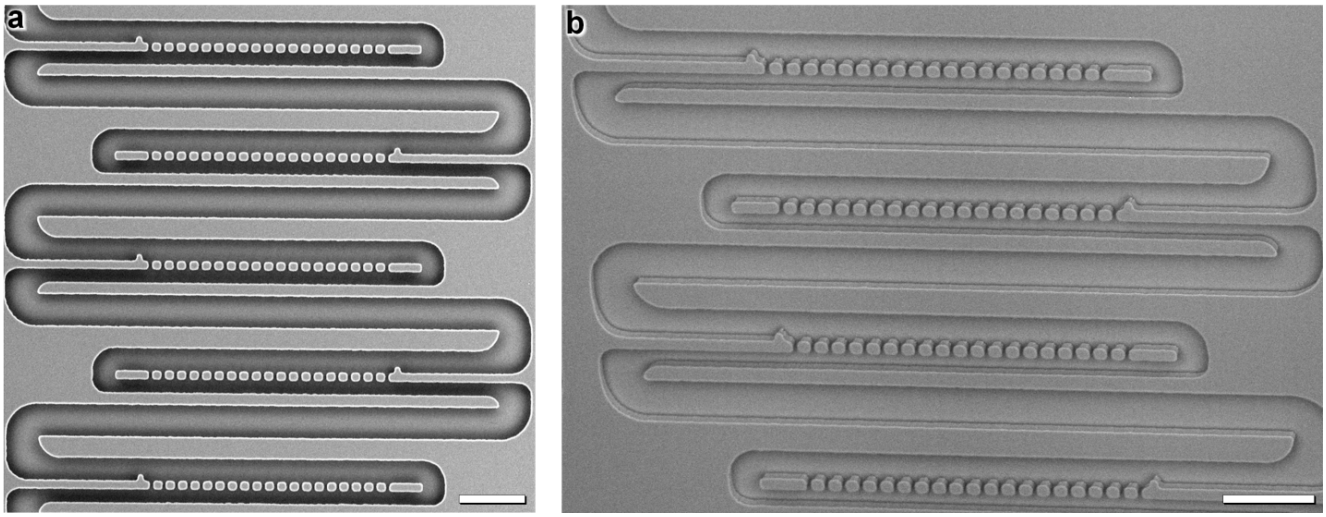

ESI Fig. 4 SEM micrographs of the resettable μPAT system (W_T = 35 μm; W_R = 20 μm). (a) Top view. (b) 30° view. Scale Bars = 100 μm.

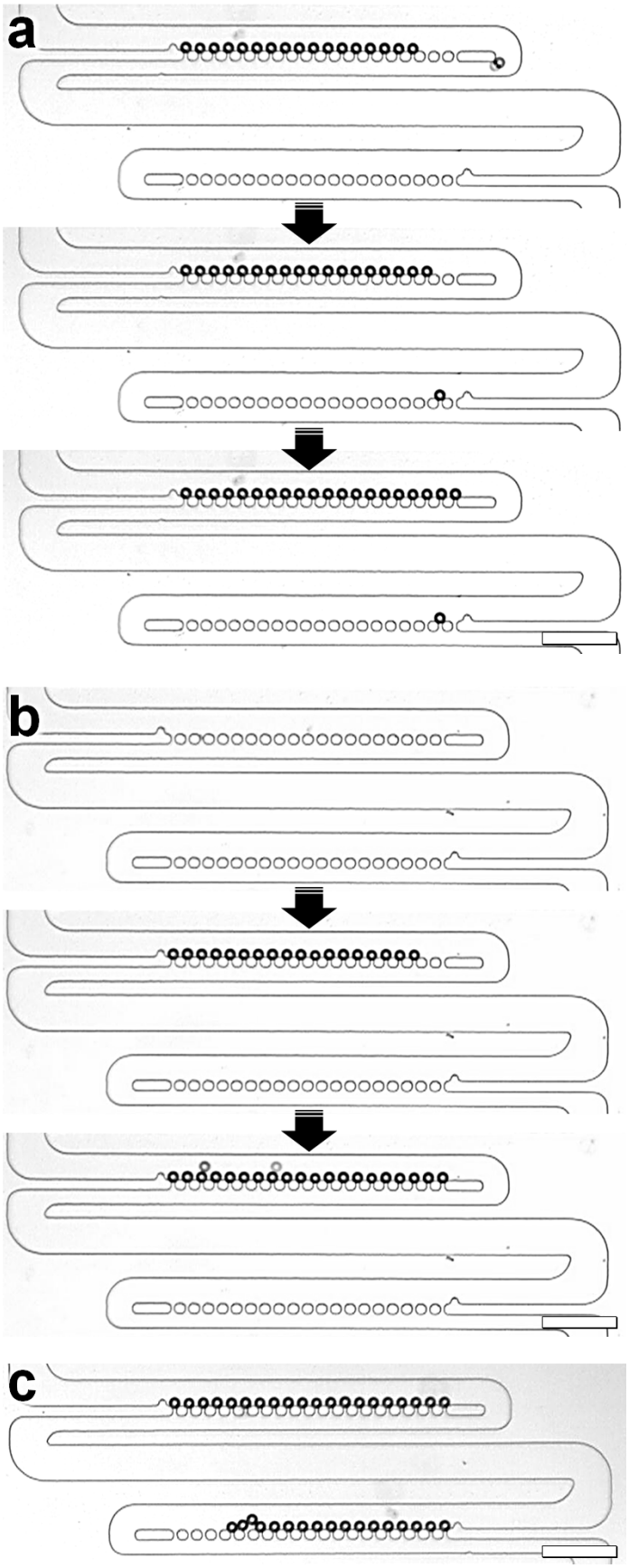

ESI Fig. 5 Example micrographs for trapping efficiency (*TE*) and loading efficiency (*LE*) quantification. (a) Sequential micrographs showing a *LE* of 95%, corresponding to 19 of 20 loaded microbeads trapping in the 20 potential vacant traps. (b) Sequential micrographs showing a *LE* of 100%, corresponding to 20 of 20 loaded microbeads trapping in the 20 potential vacant traps. (c) *TE*s shown are: (*top*) 100%, corresponding to 20 arrayed microbeads in 20 potential trapping sites, and (*bottom*) 65% "one bead per trap" arraying, corresponding to 13 trapped microbeads that are not in contact with other microbeads in 20 potential traps, and 75% "multiple beads per trap" arraying, corresponding to 15 trapped microbeads (*i.e.*, including two beads that are in contact with other microbeads) in 20 potential traps. Scale Bars = 100 μm.

In prior reports, terms for quantifying particulate-based arrays, such as the "releasing rate," the "trapping efficiency" (or "yield"), and the "loading efficiency," have been assigned a variety of definitions. In this work, standardized equations are presented for quantifying the efficiencies associated with resettable particulate-based arraying systems.

Microarray resettability was evaluated using two different efficiencies. First, microbead suspensions were loaded *via* the outlet (*i.e.*, opposite the direction of particle loading) to quantify the resetting efficiency for an empty microarray (RE_E), which was calculated as:

$$RE_E = \frac{N_m}{N_L} \tag{1}$$

where N_m is the number of particles loaded *via* the outlet that remain mobile (*i.e.*, particles that are not immobilized at the backs of trapping sites), and N_L is the total number of particles loaded. In addition, a second resetting efficiency was quantified after completing the particle arraying process. The resetting efficiency for a microarray filled with previously arrayed particles (RE_F) was calculated as:

$$RE_F = \frac{N_r}{N_a} \tag{2}$$

where N_r is the number of particles that release from the microarray (*i.e.*, without being re-immobilized at the backs of trapping sites), and N_a is the total number of initially arrayed particles prior to reversing the flow polarity.

Efficiencies associated with particle arraying were also quantified. Defining the loading efficiency (*LE*) as the proportion of loaded particles that are eventually immobilized can be misleading because loading a low number of particles in a system with high numbers of potential trapping sites would produce a high efficiency. To preclude this issue, here the *LE* is calculated as:

$$LE = \frac{N_i}{N_L} \text{ for } N_L = N_T \tag{4}$$

where N_i is the number of particles immobilized, and N_L is the number of particles loaded – with the condition that the number of particles loaded (N_L) is equivalent to the number of potential trapping sites that could have been occupied (N_T). For the resettable μPAT system, both N_L and N_T were 20. For testing systems in which microbead clogging was observed, the *LE* was quantified as 0%. ESI Fig. 5a and b show *LE*s of 95% and 100%, respectively.

The trapping efficiency (*TE*) was calculated as:

$$TE = \frac{N_a}{N_T} \tag{3}$$

where N_a is the number of arrayed particles successfully arrayed in the designated trapping sites, and N_T is the total number of potential trapping sites that could have been occupied. "One particle per trap" arraying refers to cases in which only one particle is immobilized in a trapping site. "Multiple particles per trap" arraying refers to cases in which at least one particle is immobilized in a trapping site, such as when additional microparticles are immobilized on top of previously arrayed particles. For testing systems in which microparticle clogging was observed, the *TE* was quantified as 0%. ESI Fig. 5c shows "one bead per trap" *TE*s of 100% (*top*) and 65% (*bottom*), and "multiple beads per trap" *TE*s of 100% (*top*) and 75% (*bottom*).

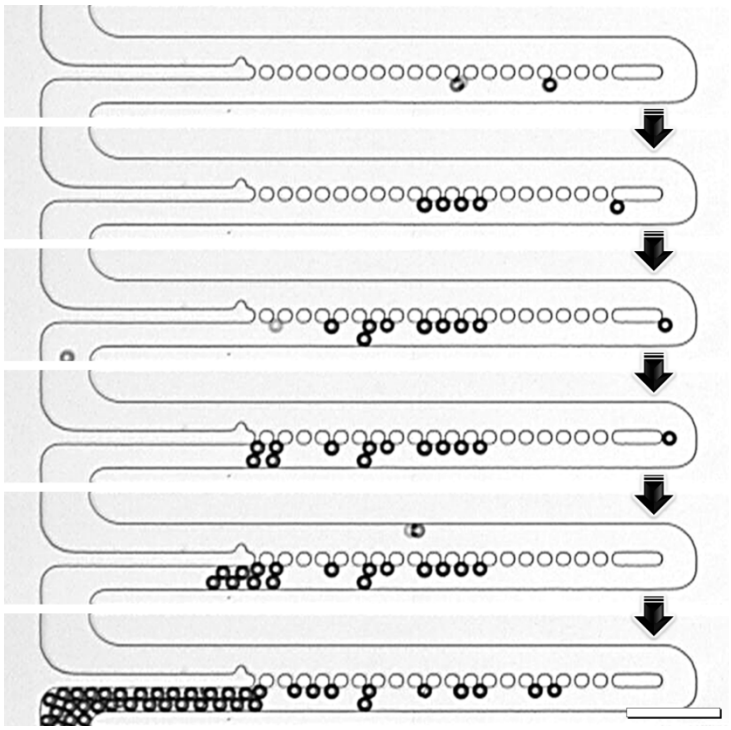

ESI Fig. 6 Experimental results for a testing system with W_R = 25 μm. Sequential micrographs of one microbead (15 μm in diameter) bypassing the backs of the trapping sites while subsequent microbeads array at the backs of the trapping sites, resulting in the formation of a microbead clog.

ESI Video Captions

All videos were generated from sequential micrographs captured every 2 to 10 seconds at 100X magnification with an epifluorescent inverted microscope (Motic AE31, Motic Instruments, Inc., Richmond, BC, Canada) connected to a Micropublisher 5.0 RTV charge-coupled device (CCD) camera (QImaging, Burnaby, BC, Canada), which was calibrated using QCapturePro (QImaging).

ESI Video 1 Sequential micrographs showing the reverse flow loading of suspended streptavidin-coated polystyrene microbeads (15 μm in diameter), which bypass the backs of the trapping sites in the resettable μPAT systems (W_T = 35 μm; W_R = 20 μm).

ESI Video 2 Sequential micrographs showing the forward flow loading of 100 microbeads into 100 designated array positions in resettable μPAT systems (W_T = 35 μm; W_R = 20 μm).

ESI Video 3 Sequential micrographs showing microarray resettability for 100 arrayed microbeads in resettable μPAT systems (W_T = 35 μm; W_R = 20 μm). From 0 to 3 seconds, the syringe pump-controlled pressure is released, which results in initial backflow (*i.e.*, reverse flow) and partial microbead release. From 3 to 3.5 seconds, the catheter coupler (*i.e.*, for inputting the microbead suspension) is removed from the inlet port, which produces additional backflow. From 3.5 to 5 seconds, the catheter coupler for inputting DI water is gradually inserted into the outlet port, which increases the reverse flow. At approximately 5 seconds, the syringe pump is set at 1.5 μl min^{-1} to release the remaining microbeads and reset the microarray. *Note:* Inserting and removing catheter couplers resulted in slight changes in the light intensity, focus, and positioning of the device.

ESI Video 4 Sequential micrographs showing the forward flow loading of suspended endothelial cells in resettable μPAT systems (W_T = 35 μm; W_R = 20 μm).

ESI Video 5 Sequential micrographs showing microarray resettability for 100 arrayed microbeads in resettable μPAT systems (W_T = 35 μm; W_R = 20 μm). From 0 to 1 seconds, the syringe pump-controlled pressure is released and the catheter coupler (*i.e.*, for inputting the cell suspension) is removed from the inlet port, both resulting in backflow. After 1 second, the catheter coupler for inputting 0.5X Trypsin is inserted into the outlet port and the syringe pump is set at 1.5 μl min^{-1} to release the remaining cells from the microarray. *Note:* Inserting and removing catheter couplers resulted in slight changes in the light intensity, focus, and positioning of the device, which limited the visibility of the cells at certain points during the releasing process.